JACS
JOURNAL OF THE AMERICAN CHEMICAL SOCIETY

COMMUNICATION

pubs.acs.org/JACS

DNA Directed Self-Assembly of Anisotropic Plasmonic Nanostructures

Suchetan Pal,[†,‡] Zhengtao Deng,[†] Haining Wang,[§] Shengli Zou,[§] Yan Liu,[*,†,‡] and Hao Yan[*,†,‡]

[†]The Biodesign Institute, [‡]Department of Chemistry and Biochemistry, Arizona State University, Tempe, Arizona 85287, United States
[§]Department of Chemistry, University of Central Florida, Orlando, Florida 32816, United States

Supporting Information

ABSTRACT: Programmable positioning of one-dimensional (1D) gold nanorods (AuNRs) was achieved by DNA directed self-assembly. AuNR dimer structures with various predetermined inter-rod angles and relative distances were constructed with high efficiency. These discrete anisotropic metallic nanostructures exhibit unique plasmonic properties, as measured experimentally and simulated by the discrete dipole approximation method.

Anisotropic nanomaterials such as gold nanorods possess unique optical properties, including a high optical extinction cross section in the range of visible and near-infrared (NIR) wavelengths, and strong localized plasmonic fields at the tips of the materials.[1,2] Due to these unique optoelectronic properties, one-dimensional (1D) gold nanorods (AuNRs) have been used for cellular imaging, cancer therapy, and biosensing.[3] Higher order assembly of AuNRs may lead to new optical properties depending on the ensuing geometric properties including size, distance, and orientation, as proposed by theory and verified by experiment.[4] Most recent attempts to create high order AuNR nanostructures have focused on the use of top-down e-beam lithography to pattern or manipulate the materials in a serial fashion.[5] New strategies are needed to deterministically position these anisotropic nanostructures in a massively parallel fashion, within complex multicomponent architectures.

Herein we report a bottom-up method to construct discrete, well-ordered AuNR and AuNR-AuNP hybrid nanoarchitectures. The nanomaterials are scaffolded by self-assembling triangular DNA origami structures,[6] with AuNR and AuNP conjugated (thiolated) DNA strands serving as the building blocks. The inter-rod angles and distances are controlled by the directed self-assembly of the materials by the underlying DNA scaffold. This work opens the door to study the collective opteoelectrical properties resulting from higher order structures of anisotropic metallic nanomaterials, as evidenced by the preliminary optical study described below.

DNA origami technology[6] is a method to create fully addressable nanostructures using ∼200 short DNA staple strands to fold single-stranded genomic DNA (e.g., DNA of M13mp18, 7249 nucleotides long) into geometrically defined nanopatterns.[7,8] DNA origami has been used to organize various spherical metallic and semiconducting nanoparticles into defined architectures.[7,9] However, using DNA scaffolds to direct the assembly of anisotropic metal nanostructures into spatially addressable higher order structures still remains an important challenge. Figure 1 illustrates our process of fabricating discrete dimeric AuNR structures using an equilateral triangle origami scaffold (∼116 nm per arm). The AuNRs were synthesized using the reported seed mediated method,[10] functionalized with the applicable DNA sequences (thiolated T_{15} or a random sequence; see Supporting Information (SI) for details) using a previously described method[11] and characterized by transmission electron microscopy (TEM) imaging. AuNRs have an aspect ratio of ∼4 with an average diameter of 12 ± 3.5 nm and average length of ∼42.5 ± 6.5 nm. They exhibit a longitudinal plasmonic band at ∼785 nm and a transverse plasmonic band at ∼520 nm (Figure S1). To facilitate the precise positioning of the AuNRs on the DNA nanostructures, selected staples were modified with sequences complementary to the single-stranded DNA displayed on the surface of the AuNRs. The staple extensions (capture probes) served to capture particular AuNRs and secure their position within the superstructure.

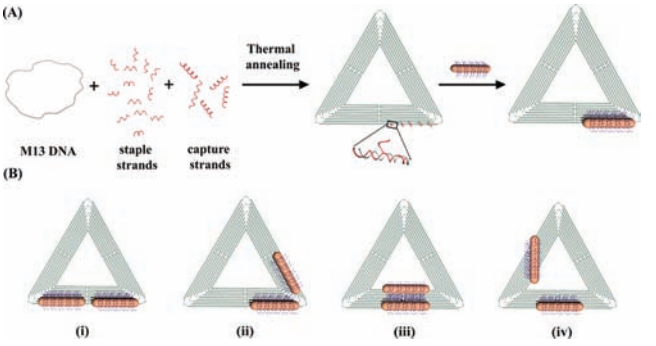

Figure 1. (A) Schematic representation of the triangular origami-NR structure assembly process. Step 1 includes thermal annealing of M13 DNA with staple and capture strands. Step 2 consists of hybridization of DNA functionalized AuNRs with complementary probe strands displayed at the origami surface to obtain site-specific immobilization of the AuNR. (B) Schematic representation of the four AuNR dimer structures with various angles between the AuNRs: (i) 180°, (ii) 60°, (iii) 0°, and (iv) 90°, respectively.

First, the efficiency of immobilizing a single AuNR on the triangular DNA origami was evaluated and the assembly process was optimized. In this case, five selected staple strands were extended with an A_{15} sequence at the 5′-end and sequentially arranged (linearly) along one arm of the triangle (Figure1A) with an interprobe distance of ∼10.4 nm (32 bps between adjacent probes). The formation of the desired origami structure was verified by TEM (Figure S1), and samples were subsequently purified by Microcon centrifugal devices with a 100 kD molecular weight cutoff filter. A 1:2 molar ratio of DNA origami:AuNRs was employed ([DNA origami] = 3 nM); the temperature of the

Received: August 20, 2011
Published: October 08, 2011

origami-AuNR solution was cycled 4 times from 45 to 30 °C, at 0.1 °C/min, to ensure complete hybridization between the DNAs displayed from the AuNRs and the capture probes extended from the DNA origami scaffold. The resulting solution mixture contained an excess of unhybridized AuNRs, the intended structure (a single DNA origami coupled to a single AuNR), and additional cross-linked structures (a single AuNR associated with two or more DNA origami) (e.g., see Figure S22). To separate the products, the sample was subjected to agarose gel electrophoresis (Figure S2). In a 1% gel, triangular shaped DNA origami with a single AuNR bound has reduced mobility compared to unbound origami. The band corresponding to singly bound origami was excised and extracted from the gel using a Freeze-n-squeeze column (Biorad Inc.) and imaged by TEM. The samples were negatively stained with 0.7% Uranyl formate and deposited on a TEM grid before imaging.

The TEM images in Figure 2 demonstrate the successful incorporation of a single AuNR on the DNA origami triangle, parallel to one arm of the structure. The AuNRs are aligned precisely as anticipated by the design of the capture strands. Spanning a distance of ~42 nm, the five capture strands are sufficient to fix the translational and rotational freedom of the AuNRs with respect to the origami template. The assembly was further characterized using high-angle annular dark field-scanning transmission electron microscopy (HAADF-STEM), which has the advantage of high image contrast and resolution. STEM, in combination with energy dispersive X-ray spectroscopy (EDS) analysis, confirmed the elemental composition of the nanostructures.

We further confirmed that the AuNRs can be immobilized in other arbitrary (not parallel to the arm) directions with respect to the triangular origami by simply redesigning the capture probe positions. For example, when a line of five capture probes was designed to form a 30° angle with the linear arm from which it was displayed, the observed products were very close to the anticipated design. The AuNRs were attached to the DNA origami with an average angle of ~30° ± 7° with respect to the underlying arm (Figures 2B and S5).

Motivated by the high efficiency and considerable level of control over the position and relative angle of a single AuNR on a DNA origami scaffold, we also designed a number of discrete dimeric structures (Figure 1B). Several designs in which the two AuNRs were related by unique angles were assembled. To fabricate the dimeric assemblies, two different sets (C_1 and C_2) of five capture strands were designed. One set (C_1) employed an A_{15} capture sequence, the same used for the monomeric structures. The other set (C_2) utilized a random probe sequence (12 nts; see SI for details), complementary to the DNA (C_2') displayed on the surface of a second group of AuNRs. Four different relative angles between the probe sets were designed: 180° (for end to end AuNR organization), 0° (for parallel AuNR organization), 90°, and 60°, respectively (Figure 1B). The preassembled triangular origami was purified to remove excess staple strands and subsequently mixed with the two groups of AuNRs (functionalized with T_{15} and C_2') in a 1:2:2 molar ratio (see SI for experimental details). 0.5xTAE-Mg^{2+} buffer was used to minimize any cross-linking or aggregation of DNA origami (a relatively low concentration of magnesium ions). The mixture was then cycled 45−30 °C four times at 0.1 °C/min. The solution was subsequently subjected to agarose gel electrophoresis, and the band corresponding to the dimeric structure (Figure S2) was carefully excised and extracted from the gel using a previously described protocol.

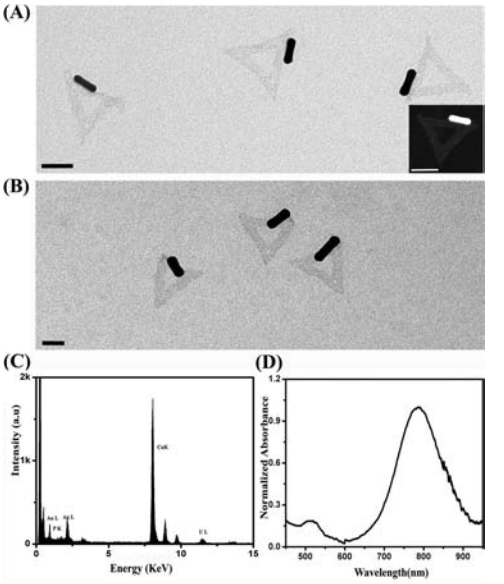

Figure 2. (A) Negatively stained TEM image (inset: STEM image) of single AuNRs immobilized at specific sites, parallel to one arm of the triangular origami scaffold. (B) Negatively stained TEM image of single AuNRs immobilized at specific sites, with a 30° angle between the NR and the arm of triangular origami. Scale bar is 50 nm. (C) EDS spectra of a AuNR DNA origami structure. The source of the Au signal is the NR, and the P signal is from the DNA origami. The U is attributed to the uranyl formate stain while the Cu corresponds to the TEM grid. (D) UV−vis−NIR spectra of a monomeric structure showing longitudinal plasmon resonance at ~788 nm and transverse plasmon resonance at ~520 nm.

The formation and angle distribution of the AuNR dimers were evaluated by TEM imaging (Figure 3B). The yield of each dimer structure was 70−80% (Table 1). The remaining 20−30% of the structures were either deformed or aggregated, presumably due to the adverse effects of multiple centrifugation steps in the purification process. The observed angles between the longitudinal axis of the two nanorods were close to the designed angles, as determined by evaluation of 100 different dimer structures found in various TEM images. Some deviation from the designed angles was observed (Table 1), which may be caused by two factors: (1) The DNA origami scaffold has intrinsic curvature, although it is designed to be flat, and (2) the surface of the TEM grid may not be perfectly flat, and the thus the origami are not perpendicular to the electron beam during imaging which could distort the observed angles.

We carried out UV−vis spectral analysis of each of the gel purified structures described above. Monomeric constructs show a longitudinal plasmonic resonance (LSPR) peak at 786 nm. In contrast, we observed a red shift of the LSPR peak for constructs (i) and (ii) by ~9 and ~6 nm, respectively (Figure 3D). Interestingly, we observed an ~5.5 nm blue shift for construct (iii) and almost no shift for construct (iv).

Theoretical simulations of the optical spectra corresponding to each of the AuNR dimer constructs were performed using the discrete dipole approximation (DDA) method.[12] For all simulations, the length and diameter of the AuNRs were assumed to be the same as observed experimentally. The inter-rod distance used in the simulations was also obtained from the experimental data. The size distribution and random orientation of single rods and dimers in solution were also considered. Finally, the dielectric constants of Au were acquired from Palik's handbook.[13]

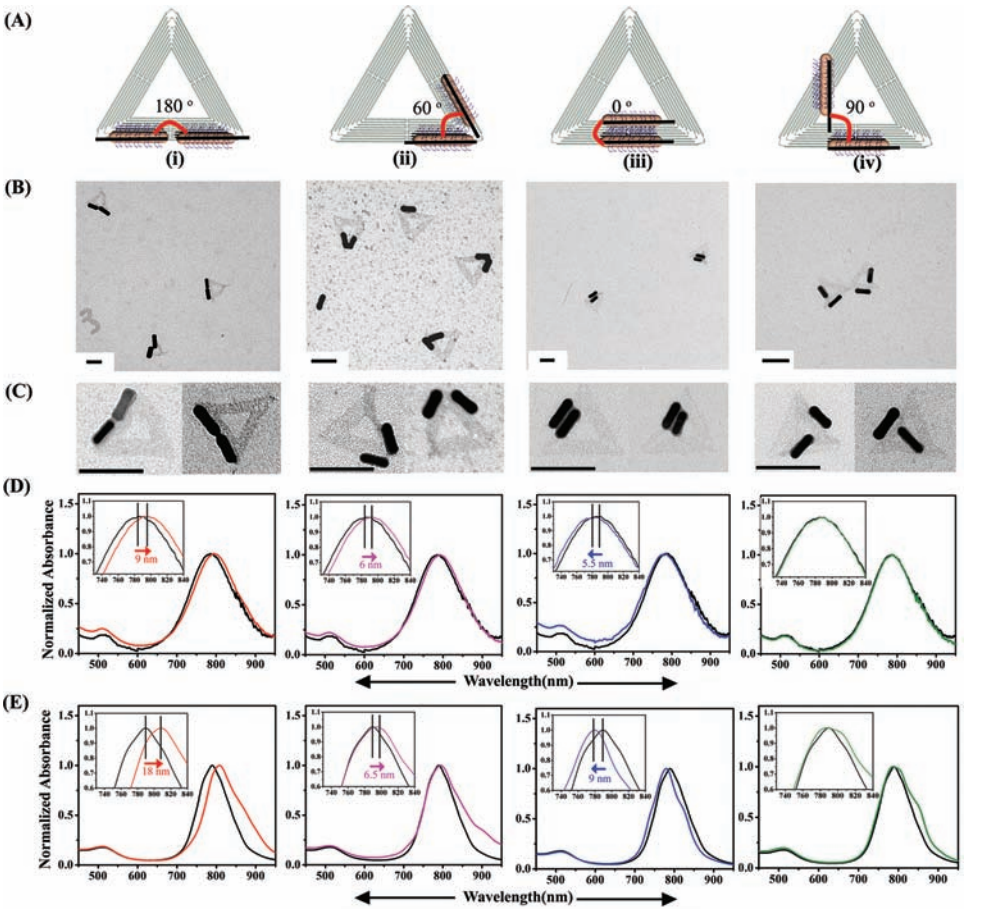

Figure 3. (A) (i)−(iv) Schematic representation of each dimer construct with the inter-rod angle indicated. (B) Representative zoom-out TEM images of each dimer construct. The samples were stained with 0.7% uranyl formate solution. (C) Representative zoom-in images revealing the precise organization of the NRs by the triangular origami structure. All scale bars are 100 nm. (D) UV−vis spectrum of the purified dimer constructs (colored curves) compared to monomeric constructs (black curve). Constructs (i), red curve, and (ii), pink curve, are red-shifted 9 and 6 nm, respectively. Construct (iii) is blue-shifted by 5.5 nm. (iv) is not shifted with respect to the monomermeric construct. (E) Simulated UV−vis spectrum corresponding to (i)−(iv) and the spectra shown in D.

The first panel (leftmost) in Figure 3E shows the predicted extinction spectrum of two parallel AuNRs with a 180° inter-rod angle and 6 nm end to end distance, compared to a single AuNR. The resonance peak appears at 790 nm for the single rod and 808 nm for the dimer, with an 18 nm red shift. The predicted shift is slightly larger than the observed 9 nm shift. The difference could be the result of a smaller size distribution in the simulations, where only three different lengths and diameters were simulated (for a total of 9 different variations of the single rod). For the construct with an inter-rod angle and distance of 60° and 5 nm, respectively, as shown in the second panel of Figure 3E, the simulated resonance peak of the NR dimer exhibited a 6.5 nm red shift, close to the experimentally measured 6 nm shift. The third panel in Figure 3E shows the simulated extinction spectrum of a AuNR dimer with a 0° inter-rod angle and an 8 nm end to end distance. The resonance wavelength of the dimer is 780 nm, which represents a 9 nm blue shift compared to that of a single rod. When two rods were organized into a perpendicular arrangement with a 16 nm separation, the resonance peak of the dimer occurred at 787 nm (right panel, Figure 3E) which is close to the resonance peak of a single rod. Overall, the predicted peak shifts correspond closely with the experimentally measured spectra for all four AuNR dimer constructs. Presumably, any discrepancies may be the result of slightly reduced yields (<100%) and possible degradation/distortion of the structures after purification. In the future, single particle microscopic and spectral characterization methods (ideally topographical imaging combined with simultaneous spectral detection) may reduce the discrepancy between simulated and experimental results.

Table 1. Assembly Yields after Purification and the Designed and Observed Angles between Components in Each of the Four Dimer Structures[a]

Sample	Yield (%)	Designed angle (deg)	Observed angle (deg)	Designed distance (nm)	Observed distance (nm)
(i)	72	180	180 ± 5	5.2	6.1 ± 4.5
(ii)	77	60	63 ± 9	3	5.0 ± 3.5
(iii)	74	0	2 ± 2	6	8.0 ± 6.0
(iv)	81	90	87 ± 8	15	16.0 ± 7.0

[a] Sample size is 100, and ± represents standard deviation of the measured parameters.

dx.doi.org/10.1021/ja207898r |J. Am. Chem. Soc. 2011, 133, 17606–17609

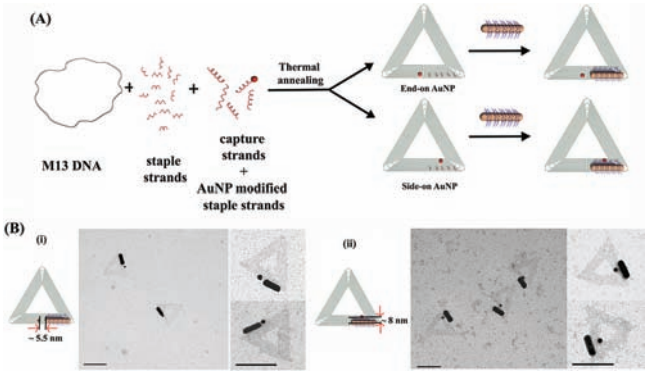

Figure 4. (A) Schematic of side-on and end-on AuNR-AuNP heterodimer structure formation. (B) Schematic diagrams and TEM images of end-on (i) and side-on (ii) AuNR-AuNP heterodimers. Scales bars are 100 nm.

Nevertheless, the directed self-assembly strategy demonstrated here is a promising method to construct and study higher order metallic nanostructures.

One of the potential applications of a DNA directed AuNR architecture is to study the interaction between anisotropic NRs and other molecules or nanoparticles. In particular, the nonuniform distribution of the electric field around the NR may influence the behavior of a nearby particle such as a fluorescent dye. Toward this end, a series of AuNP/AuNR heterodimer structures were designed and constructed. A 10 nm AuNP was placed in close proximity to an AuNR on an underlying triangular DNA origami scaffold, demonstrating the programmability of DNA directed assembly and ability to create asymmetric metallic nanoarchitectures.

The arrangement of AuNPs with respect to the AuNR (side-on or end-on) was predefined by modifying a selected staple strand on the origami with a thiol group (Figure 4A). The 10 nm AuNP was conjugated to this staple strand using a 1:1 ratio between NP and staple.[14] The conjugate was subsequently mixed with M13 and a set of additional staple strands, including five A_{15} modified capture strands for AuNR immobilization, in a 1:1:5 ratio. The assembled origami structure, with a single AuNP displayed at the desired location, was assembled with very high yield of ~95% (Figures S15−S16, S19−S20). The construct was purified using a Microcon centrifugal device (100 kD MWCO) to remove any excess staple strands, was subsequently mixed with T_{15} DNA functionalized AuNRs in a 1:2 ratio, annealed, and gel purified before TEM imaging.

Figure 4B contains representative images of the end-on and side-on heterodimer constructs, respectively. The results show that both the orientation and distance between the 10 nm AuNP and AuNR can be precisely controlled using a DNA origami scaffold. For example, the expected distance between the AuNP and AuNR in the end-on design was ~5.5 nm (design shown in SI), and the measured distance was 8 ± 4 nm. Similarly, the distance between the AuNP and AuNR in the side-on design was predicted to be ~8 nm, while the measured distance was 10 ± 5 nm. The small differences between the observed and expected distances are likely the result of uncertainty in the actual size of the AuNRs (~10% variance in both dimensions) and the flexibility of the 15 base pair capture strand.

In summary, we have developed a robust and programmable strategy to immobilize and orient AuNRs (12 × 42 nm^2) at specific positions on a DNA origami scaffold. This method was extended to assemble a number of different AuNR dimer structures, with predefined angles between metallic components. We also demonstrated the spatial symmetry of the metallic particles can be interrupted by precisely orienting the components on the underlying DNA scaffold. This strategy overcomes the challenging problem of site-specific placement of a single particle or molecule close to a single AuNR, and will open new avenues to characterize the effect of interparticle distance and geometrically dependent photonic interactions between AuNRs and other nanophotonic elements, such as molecular fluorophores, quantum dots, and other plasmonic nanoparticles. Future studies are needed to scale up this strategy to template longer rods and larger particles with precision.

■ ASSOCIATED CONTENT

Supporting Information. Material and methods, designs and DNA sequences, additional TEM images, UV−vis spectrum. This material is available free of charge via the Internet at http://pubs.acs.org.

■ AUTHOR INFORMATION

Corresponding Author
yan_liu@asu.edu; hao.yan@asu.edu

■ ACKNOWLEDGMENT

This research was partly supported by grants from the ONR, ARO, and NSF to Y.L. and from the ONR, ARO, NSF, and Sloan Research Foundation to H.Y. The authors acknowledge the use of EM facility in School of Life Science at Arizona State University. S.Z. thanks the NSF, ONR, and ACS/PRF for the support of research. We thank Jeanette Nangreave for proofreading the text.

■ REFERENCES

(1) Burda, C.; Chen, X. B.; Narayanan, R.; El-Sayed, M. A. *Chem. Rev.* **2005**, *105*, 1025–1102.
(2) Huang, X. H.; Neretina, S.; El-Sayed, M. A. *Adv. Mater.* **2009**, *21*, 4880–4910.
(3) (a) Yu, C.; Irudayaraj, J. *Biophys. J.* **2007**, *93*, 3684–3692. (b) Yu, C.; Nakshatri, H; Irudayaraj, J. *Nano Lett.* **2007**, *7* (8), 2300–2306. (c) Wang, L.; Zhu, Y.; Xu, L.; Chen, W.; Kuang, H.; Liu, L.; Agarwal, A.; Xu, C.; Kotov, N. A. *Angew. Chem., Int. Ed.* **2010**, *49* (32), 5472–5475. (d) Dickerson, E. B.; Dreaden, E. C.; Huang, X.; El-Sayed, I. H.; Chu, H.; Pushpanketh, S.; McDonald, J. F.; El-Sayed, M. A. *Cancer Lett.* **2008**, *269*, 57–66.
(4) Li, Y.; Qian, F.; Xiang, J.; Lieber, C. M. *Mater. Today* **2006**, *9*, 18–27.
(5) Lu, W.; Lieber, C. M. *J. Phys. D: Appl. Phys.* **2006**, *39*, R387–R406.
(6) Rothemund, P. W. K. *Nature* **2006**, *440*, 297–302.
(7) Nangreave, J.; Han, D.; Liu, Y.; Yan, H. *Curr. Opin. Chem. Biol.* **2010**, *14*, 608–615.
(8) Shih, W. M.; Lin, C. *Curr. Opin. Struct. Biol.* **2010**, *20*, 276–282.
(9) Tan, S. J.; Campolongo, M. J.; Luo, D.; Cheng, W. *Nat. Nanotechnol.* **2011**, *6*, 268–276.
(10) Nikoobakht, B.; El-Sayed, M. A. *Chem. Mater.* **2003**, *15*, 1957–1962.
(11) Jones, M. R.; Macfarlane, R. J.; Lee, B.; Zhang, J. A.; Young, K. L.; Senesi, A. J.; Mirkin, C. A. *Nat. Mater.* **2010**, *9*, 913–917.
(12) (a) Purcell, E. M.; PennyPacker, C. R. *Astrophys. J.* **1973**, *186*, 705–714. (b) Draine, B. T. *Astrophys. J.* **1988**, *333*, 848–872.
(13) Palik, E. D. *Handbook of Optical Constants of Solids*; Academic Press: New York, 1985.
(14) Sharma, J.; Chhabra, R.; Anderson, C. S.; Gothelf, K. V.; Yan, H.; Liu, Y. *J. Am. Chem. Soc.* **2008**, *130*, 7820–2821.